Generative Design of Bionic Structures Via Concurrent Multiscale Topology Optimization and Conformal Geometry Method

Long Jiang
Department of Mechanical Engineering,
State University of New York,
Stony Brook, NY 11794
e-mail: ljiang72@ford.com

Xianfeng David Gu
Department of Computer Science,
State University of New York,
Stony Brook, NY 11794;
Department of Applied
Mathematics and Statistics,
State University of New York,
Stony Brook, NY 11794
e-mail: gu@cs.stonybrook.edu

Shikui Chen[1]
Department of Mechanical Engineering,
State University of New York,
Stony Brook, NY 11794
e-mail: shikui.chen@stonybrook.edu

Topology optimization has been proved to be an efficient tool for structural design. In recent years, the focus of structural topology optimization has been shifting from single material continuum structures to multimaterial and multiscale structures. This paper aims at devising a numerical scheme for designing bionic structures by combining a two-stage parametric level set topology optimization with the conformal mapping method. At the first stage, the macro-structural topology and the effective material properties are optimized simultaneously. At the second stage, another structural topology optimization is carried out to identify the exact layout of the metamaterial at the mesoscale. The achieved structure and metamaterial designs are further synthesized to form a multiscale structure using conformal mapping, which mimics the bionic structures with "orderly chaos" features. In this research, a multi-control-point conformal mapping (MCM) based on Ricci flow is proposed. Compared with conventional conformal mapping with only four control points, the proposed MCM scheme can provide more flexibility and adaptivity in handling complex geometries. To make the effective mechanical properties of the metamaterials invariant after conformal mapping, a variable-thickness structure method is proposed. Three 2D numerical examples using MCM schemes are presented, and their results and performances are compared. The achieved multimaterial multiscale structure models are characterized by the "orderly chaos" features of bionic structures while possessing the desired performance.
[DOI: 10.1115/1.4047345]

Keywords: computational geometry, computer-aided engineering, conceptual design, design automation

1 Introduction

Geometry and material are two essential factors of the structural design. Compared with single material structures, a multimaterial structure can have a better performance under many conditions [1] and can make some design objectives easier to be achieved [2]. Besides natural materials, the emergence of metamaterials has significantly expanded the range of materials accessible to engineers. Metamaterials can offer possibilities that cannot be achieved by natural materials [3–7]. With the rapid development of structural optimization and additive technology, designing multiscale structures with space-varying metamaterials has become accessible [8–10]. There is a growing need for a computational framework for the generative design of multimaterial structures at multiple scales.

Topology optimization is a powerful and advanced structural designing tool. There are several different approaches in this field, and a comparative review regarding different approaches can be found in Ref. [11]. Among those, the level set approach stands out for its flexibility in handling topological changes with clear design boundaries for different engineering applications [12–17]. Generally, by using the zero-level set of the level set function to model the structural design boundary [18], one level set function can divide the design domain into three parts: the void domain, the material domain, and the boundary or interface between them. When two or multiple material phases are involved, the "color" level set method [19,20], the piecewise constant level set method [21], and the reconciled level set method [22] are the widely

used schemes within the level set framework. Specifically, similar to generating new colors by mixing primary colors, the "color" level set method can use n level set functions to represent up to 2^n different regions. Therefore, each region can be considered possessing a given property for structural topology optimization. In the current framework, this scheme is utilized for a better multimaterial handling potential.

Compared with monoscale structures, multiscale structures possess mesoscale fillings with fine-tuned properties at a low overall density [23–25]. Therefore, they can be found in a wide range of engineering applications [26]. In the designing of multiscale structures, the key issues are how to find the constitutive metamaterials with desired properties, and how to assemble the multiscale structures [27,28]. Within the level set framework, a series of metamaterial designs have been reported, such as designing negative permeability metamaterials [29], negative Poisson's ratio metamaterials [30,31], electromagnetic metamaterials [7], zero or negative thermal expansion metamaterials [32], and so on. However, designers can not fully explore the potential of the multiscale structure by only designing the metamaterial infill. Ideally, the mesoscale structures and the macroscale structures should be designed in a concurrent manner since the macroscopic loading and boundary conditions will affect not only the macroscale overall structural layout but also the metamaterial properties at different locations. A density-based approach for concurrently designing multiscale porous structures was reported by Deng and Chen [33], where the solid isotropic material with penalization (SIMP) method was used to optimize the microscale structure, and the porous anisotropic material with penalization (PAMP) method is used to optimize the macroscale structure. Sivapuram et al. [34] developed the concurrent structural topology optimization for multiscale structures where the mesoscale metamaterials have fixed

pre-defined locations. Wang et al. [35] proposed the concurrent design of multiscale structures filled with spatially varying graded microstructures to ensure the connectivity between adjacent meso-scale units. Both Sivapuram's work with predefined metamaterial locations and Wang's work with similar topological feature meta-materials are meant to alleviate the high computational cost of intro-ducing too many different types of metamaterials in different regions. Another approach for the concurrent design of the multi-scale structure is proposed by Li et al. [36], where the density-based method is employed in the macroscale, and the level set approach is employed in the mesoscale. The mesoscale metamaterial is deter-mined by the intermediate density generated from the macroscale optimization. This combination converts the undesired intermediate densities of the density-based approach into an advantage of the entire design methodology, and the numerical examples have veri-fied the effectiveness of this process.

However, some numerical drawbacks exist in the conventional level set structural topology optimization framework [37,38]. A promising solution is to extend it to the parameterized level set method (PLSM) [39]. In the PLSM framework, combined with mathematical programming and the gradient-based optimizer MMA [40], introducing multiple design constraints can be straight-forward. The PLSM also can generate new holes during the optimi-zation to add extra flexibility and robustness to the optimization [37]. Some other level-set-based approaches that can handle multi-ple design constraints and design variables are reported in Refs. [41,42]. The optimized structure generated via PLSM has also been reported to have the advantage of requiring less prefabrication time for the additive manufacturing of the final design [43], which is a preferred feature for bridging the gap between designing and applications.

In this paper, the cardinal basis function (CBF) replaces the RBF kernel function [44,45] so that the CBF-based level set topol-ogy optimization framework for multimaterial and multiscale struc-ture design is formulated [46–48]. The multimaterial structure is modeled by the "color" level set approach. At the macro-scale, the overall structural topology and the corresponding effective metamaterial properties are optimized simultaneously. Using the optimized effective metamaterial properties as targets, a second-stage topology optimization is carried out to find out the metamater-ial structural layout [49–51]. A distance regularization energy functional [52] is used to maintain the distance-regularized shape of the level set functions. For multimaterial and multiscale structure designs, apart from getting the structural topologies in different scales, how to integrate them together with high fidelity of the designed performance is another challenge. Simply trimming the metamaterial array to fit into the structure boundaries may cut through boundary unit cells, as shown in Fig. S10 available in the Supplemental Materials on the ASME Digital Collection, causing isolated or overhung structures, bringing difficulties in the analyz-ing and manufacturing process. To make the mesoscale infills con-formal to the design boundary, the angle-preserving, or local-shape-preserving, conformal mapping is employed to assem-ble the multiscale structure. Conformal mapping possesses some intrinsic advantages for metamaterial assembly. It can keep the designed thermal properties invariant by maintaining the local shape of the unit cell in the mapping process. However, when it comes to elastic properties, the conformal mapping process will introduce local rotation and uniform stretching (or contraction) to the mapped structure. In this paper, the local rotation will be handled by utilizing isotropic metamaterial unit cells. To handle the local distortion, a multi-control-point conformal mapping (MCM) method is proposed to compensate the deviation of property tensors caused by the distortion. A variable-thickness structure scheme is proposed to compensate the local stretching/compressing on the metamaterial unit cells. By utilizing these measures, the final mapped structures are expected to have performances close to the optimized design. Three MCM mapping variations, namely, the region-by-region MCM (R-MCM) with uniform thickness, the R-MCM mapped variable-thickness structure, and the all-in-one

MCM (A-MCM) mapped variable-thickness structure with variable thickness are employed and compared, aiming at preserving the designed structural performance as much as possible. The rest of this paper is structured as follows. In Sec. 2, the "color" level set method for designing multimaterial structures using the CBF-based concurrent parametric level set framework is detailed. The bench-mark examples under different mapping schemes, together with numerical verification, are listed in Sec. 3. The conclusions are drawn in Sec. 4. Regarding the conformal geometry method, the dif-ferences between different mapping approaches, and the topology optimization sensitivity analysis, the readers can be referred to the Supplemental Materials for further details.

2 The Cardinal Basis Function-Based Concurrent Topology Optimization Setup for Multiscale and Multimaterial Structural Designs

2.1 The "Color" Level Set Model for Multimaterial Representation. In the conventional level set representation with one level set function, the design boundary is implicitly described as the zero-level set of the one-higher dimensional level set function [12,13]. However, when multiple structure phases are introduced, the "color" level set representation can be utilized. With n level set functions, the design domain can be divided into up to 2^n differ-ent regions. The level set functions used can be described as follows:

$$\begin{cases} \Phi_k(\boldsymbol{x}) > 0, & (\boldsymbol{x} \in \Omega_k \smallsetminus \Gamma_k) \\ \Phi_k(\boldsymbol{x}) = 0, & (\boldsymbol{x} \in \Gamma_k), \qquad k = 1, \ldots, n \\ \Phi_k(\boldsymbol{x}) < 0, & (\boldsymbol{x} \in D \smallsetminus \Omega_k \cup \Gamma_k) \end{cases} \qquad (1)$$

In Eq. (1), Φ_k denotes the kth level set function and Ω_k, Γ_k repre-sents the region where the kth level set function has positive value and its corresponding boundary, respectively. D represents the design domain. The example of identifying different regions inside the design domain by the sign of the level set function is illus-trated in Fig. 1.

2.2 Concurrent Macroscale and Mesoscale Optimization With Cardinal Basis Function-Based PLSM. With a given kernel function at the jth node as Ψ_j, the kth level set functions for multimaterial representation can be parameterized into the fol-lowing form:

$$\Phi_k(\boldsymbol{x}) = \sum_{j=1}^{m} \Psi_j(\boldsymbol{x}) \mu_{kj}, \quad k = 1, \ldots, n \qquad (2)$$

In the conventional parametric level set method, the kernel func-tion is commonly selected as the radial basis function (RBF). However, with a given support radius, the support regions of neigh-boring RBF kernel functions will overlap with each other. There-fore, the corresponding weights, namely, μ_{kj} in Eq. (2), do not have clear upper or lower bounds. This effect can be visualized by comparing the plot of different types of kernel functions in Fig. S16. As the design variables [37], the design variable bounds should be passed to the optimizer explicitly. This issue can be solved by constructing the CBF as the kernel function, as seen in Fig. S16(b), for the level set function parameterization [44]. The CBFs have the Kronecker delta property as:

$$\Psi_j(x_i) = \begin{cases} 1, & (\text{if } i = j) \\ 0, & (\text{if } i \neq j) \end{cases} \quad j = 1, \ldots, m \qquad (3)$$

Here, m is the total node number of the parametric level set function. When the CBF is used for the level set function parameterization, the corresponding weights will be the upper and lower bounds of the level set function itself. These explicit bounds can maintain the numerical stability of the optimizer and avoid the trial and error approach for guessing those bounds.
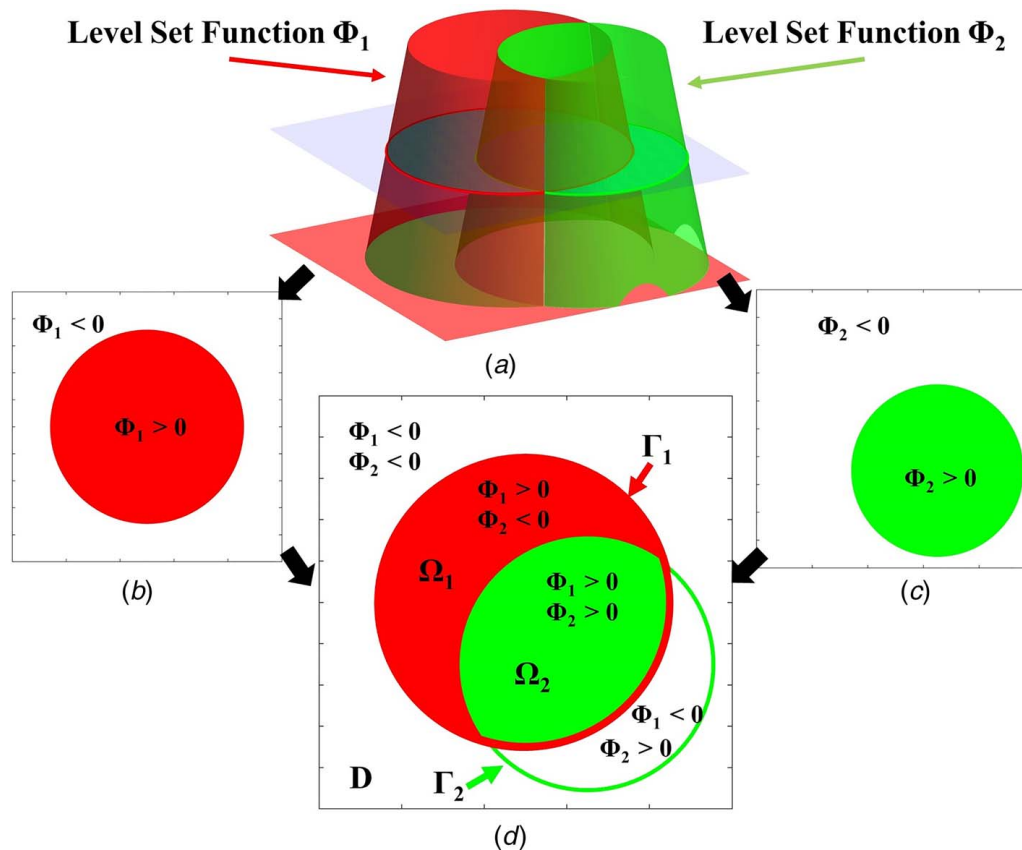
Fig. 1 The "color" level set representation. (a) The two distance-regularized level set functions. (b) The sign of level set function 1. (c) The sign of level set function 2. (d) The combination of two level set functions. In this research, Ω_1 represents the first material phase with boundary Γ_1 and Ω_2 represents the second material phase with boundary Γ_2. The reset regions are considered as void inside the design domain D. (Color version online.)

Generally, a multimaterial optimization for minimal mean structural compliance can be formulated as follows:

$$
\begin{aligned}
\text{Min:} \quad & J = \int_D \epsilon(\boldsymbol{u}) : \boldsymbol{D}^* : \epsilon(\boldsymbol{v}) d\Omega \\
\text{s.t.:} \quad & a(\boldsymbol{u}, \boldsymbol{v}, \Phi) = l(\boldsymbol{v}, \Phi) \\
& Vol_k \leq Vol_k^t, \quad (k = 1, \ldots, n) \\
& \mu_{kj}^L \leq \mu_{kj} \leq \mu_{kj}^U, \quad (j = 1, \ldots, m)
\end{aligned}
\tag{4}
$$

In Eq. (4), the $\epsilon(\boldsymbol{u}) : \boldsymbol{D}^* : \epsilon(\boldsymbol{u})$ represents the strain energy density of the structure with an elastic tensor $\boldsymbol{D}^*$ calculated from the aforementioned "color" level set multimaterial representation. In the proposed concurrent optimization framework, both the structural topology and the mesoscale metamaterial properties are optimized simultaneously. Therefore, at the end of the macro stage optimization, the optimized structural layout and the corresponding material properties can be obtained. The actual mesoscale metamaterial layout can be achieved by performing a second stage optimization. The details of the optimization setup and the sensitivity analysis can be found in the section " Sensitivity Analysis and Flowchart of the Concurrent Structural Topology Optimization" in the Supplemental Materials.

As a function of the design variable μ, the $\boldsymbol{D}^*$ will essentially be updated during the optimization process to discriminate different material phases. $\boldsymbol{u}$ is the displacement field and $\boldsymbol{v}$ is the test function. The kth material has the volume of Vol_k that is constrained by its volume target Vol_k^t. At most, the number of different material phases in "color" level set can reach to 2^n, where n is the total number of level set functions. In this paper, this is simplified to

only n different phases. The lower and upper bounds for the design variable μ_{kj} can be easily got from the upper and lower bound of the corresponding level set function. The energy bilinear form $a(\boldsymbol{u}, \boldsymbol{v}, \Phi)$ and the load linear form $l(\boldsymbol{v}, \Phi)$ are detailed as follows:

$$
\begin{aligned}
a(\boldsymbol{u}, \boldsymbol{v}, \Phi) &= \int_D \epsilon(\boldsymbol{u}) : \boldsymbol{D}^* : \epsilon(\boldsymbol{v}) d\Omega \\
l(\boldsymbol{v}, \Phi) &= \int_\Gamma \boldsymbol{t} \cdot \boldsymbol{v} d\Gamma
\end{aligned}
\tag{5}
$$

To calculate the volume for each material phase, with the Heaviside function H, the following equation can be formulated:

$$
Vol_k = \int_D \prod_{i=1}^k H(\Phi_i) d\Omega, \quad i = 1, \ldots, n
\tag{6}
$$

This volume fraction formulation can be understood in a more intuitive way. For example, when 2 level set functions are used, the total number of potential material phases can reach up to $2^2 = 4$. This is achieved by combining the positive and the negative areas of each level set function. In this paper, this potential is not fully utilized. Two level set functions are used to only represent two material phases for simplicity. The two different volumes can be calculated as follows:

$$
Vol_1 = \int_D H(\Phi_1) d\Omega, \quad Vol_2 = \int_D H(\Phi_1) H(\Phi_2) d\Omega
\tag{7}
$$

Here, Vol_1 is utilized to calculate the total structural volume. In the current research, Vol_2 is used to calculate the volume of the relatively

hard material. The soft material volume can be easily calculated by finding the difference between these two.

2.2.1 Formulation of the Metamaterial Optimization. With the optimized material properties achieved in the macroscale stage, next, the structural topology optimization of the mechanical metamaterial [47] is elaborated. In the current example, essentially, the mechanical metamaterial will be designed as porous structures with specified elasticity tensors. Although the local shapes of the unit cells are preserved by the conformal mapping, rotations can still be introduced. Therefore, the isotropic mechanical metamaterial unit cells are preferred. To enforce the isotropy of the mechanical metamaterial, an additional isotropic constraint is included in the optimization setting:

$$\text{Min:} \quad J_{meta} = \frac{1}{2} \sum_{ijkl}^{n} (C_{ijkl}^{H} - C_{ijkl}^{*})^2$$

$$\text{s.t.:} \quad \int_{D} H(\Phi) d\Omega \leq Vol_{meta}^{t} \quad (8)$$

$$a(\boldsymbol{u}, \boldsymbol{v}, \Phi) = l(\boldsymbol{v}, \Phi)$$

$$C_{1212}^{*} = (C_{1111}^{H} + C_{2222}^{H})/4 - C_{1122}^{H}/2$$

Here, Φ is the level set function for the metamaterial design, also parameterized by the CBF. The C_{ijkl}^{H} is the homogenized elasticity tensors with the targets at C^{*}_{ijkl}. The volume of the mechanical metamaterial is constrained by the volume target Vol_{meta}^{t}. The structural isotropy is ensured when the condition of $C_{1212}^{*} = (C_{1111}^{H} + C_{2222}^{H})/4 - C_{1122}^{H}/2$ is satisfied [53]. With the strain energy method [54], essentially, the effective elasticity tensor in the least square optimization can be calculated from the structural strain energies under different loading scenarios. The design variables of this optimization are still the weights for the CBF-parameterized level set function for the mechanical metamaterial designs. As for the details of the sensitivities, the readers can be referred to our previous publication [47] for further details. It needs to be pointed out that the bounds of the material properties should be selected within a reasonable limitation. In this current research, the bounds are selected using Ref. [55] as a reference where microstructures were designed to reach its maximum material properties. The topology optimization sensitivity analysis details can be found in the Supplemental Materials.

3 Numerical Examples and the Multi-Control-Point Conformal Mapping Scheme

3.1 Simultaneous Optimization of the Macroscale MBB Beam Structure and Mesoscale Metamaterials.
In this section, a multimaterial MBB beam structure is designed under proposed framework. The macroscale topology optimization boundary condition is illustrated in Fig. 3(a). A $F = 1$ force is applied at the lower center of a 2-by-1 domain with fixed lower corners. The domain is discretized into 100×50 elements. The effective Young's modulus of the soft material is given the range from 0.05 to 0.1, and the hard one is between 0.15 and 0.2. The initial effective Young's modulus values of the soft material and the hard material are given 0.075 and 0.175, respectively. The overall material volume is constrained at 60%, and the hard material volume is constrained at 30%. The Poisson's ratio for all materials is set to be 0.3. For all the numerical examples in this research, the FEA is performed under the plane-stress assumption. The upper and lower bounds for the design variables in all the numerical examples are set to be three times of the level set function grid size.

The convergence history of the optimization process is shown in Fig. 2. At the end of the macroscale topology optimization, the total and the hard material volume for the final design is 59.995% and 29.995%, respectively. The optimized effective Young's modulus for the soft metamaterial is 0.1, and the hard one is 0.2, respectively. By using these two values as targets, the second topology optimization is carried out to get the isotropic metamaterial layouts. The Young's modulus for constructing both metamaterials is the same at 1. The volume is 30% and 40% for the soft and hard metamaterials, respectively. A bounding box is introduced to the metamaterial designs to ensure the connectivity of the adjacent metamaterial unit cells. In the current framework, the bounding box thickness is selected to be a given value of 2% of the square unit cell edge length. The adding of the bounding box is a simple but straightforward way of connecting adjacent unit cells within the multiscale structure. Other potential techniques such as adding geometric connectivity conditions [56] or adding virtual forces [57] can also ensure the interface connectivity of unit cells within the level set framework. An isotropy polar plot scheme, as shown in Fig. S17, is utilized to illustrate the isotropy of the designed metamaterials. Essentially, it is plotting the metamaterial effective property constraint (the last statement in Eq. (8)) from 0 deg to 360 deg. When the metamaterial is isotropic, its orientation will not affect its effective property, so a perfectly round circle will be plotted. If the metamaterial is not isotropic as expected, this plot will
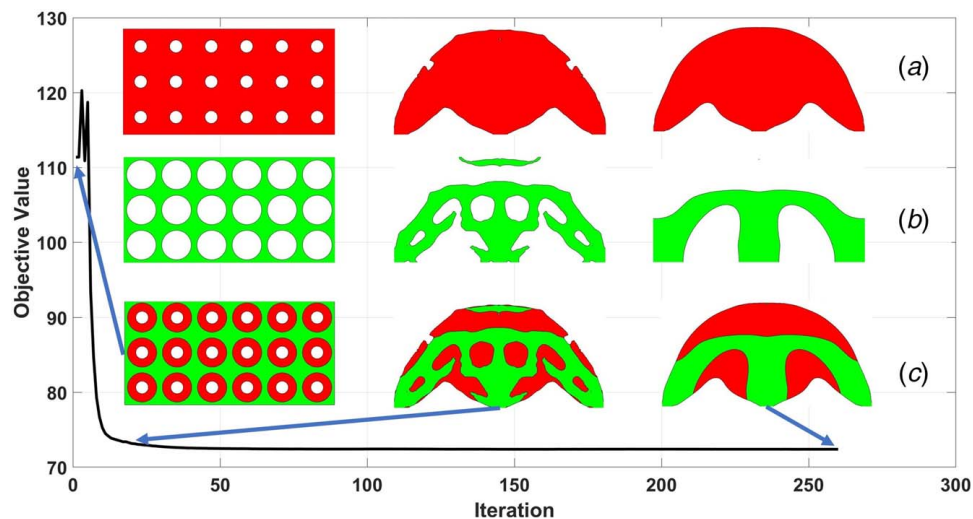

Fig. 2 The evolution history of the MBB beam structure example: (*a*) the evolution history of the first zero-level set function, (*b*) the evolution history of the second zero-level set function, and (*c*) the evolution history of the multimaterial structure. Red:soft material. Green: hard material. (Color version online.)
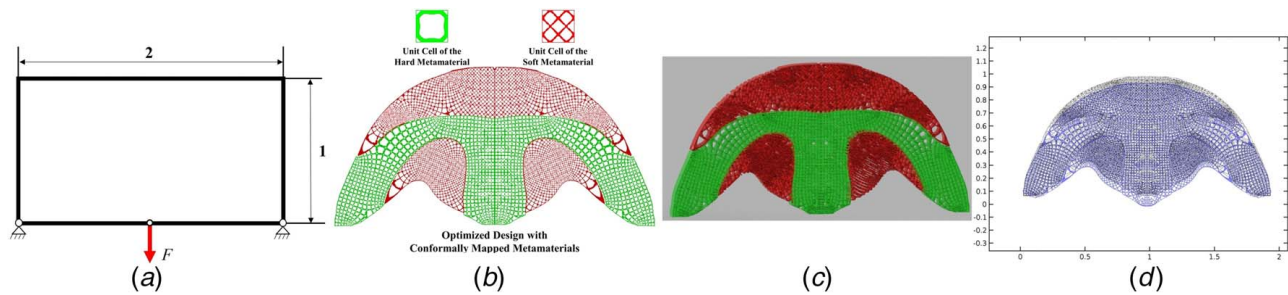
Fig. 3 (*a*) The boundary condition of the MBB beam structure example. (*b*) The R-MCM mapped MBB beam multiscale structure with conformally mapped hard (red) and soft (green) metamaterials. (*c*) The R-MCM mapped MBB beam structure CAD model with uniform thickness. (*d*) The FEA calculation of the R-MCM mapped multiscale MBB beam with uniform thickness. Black: pre-deformation structure. Blue: post-deformation structure. (Color version online.)

deviate from the reference circle to become ellipse or other types of shapes. So, this isotropic polar plot is helpful to visualize how "isotropic" the current metamaterial is. For more details about the structural isotropy polar plot, the readers are referred to Ref. [47] for further details.

3.1.1 Region-by-Region Multi-Control-Point Conformal Mapping With Uniform Thickness. Generally, to form the multiscale structure, a commonly used procedure is to assemble an array of the mesoscale metamaterial structure and trim this array to fit into the macroscale structure. This process might introduce isolated or overhung structures, bringing difficulties in structural analyzing and manufacturing. In this research, a preliminary approach is introduced to form the multiscale structures with mesoscale metamaterial unit cells conformal to the structural boundaries. This approach is made possible by utilizing the conformal geometry theory. With the preferred angle-preserving property, the conformal mapping will mathematically preserve the designed mesoscale metamaterial properties. This can ensure the high fidelity of the mapped multiscale structural performance. With different problem settings and mapping preferences, in this paper, three preliminary mapping approaches, namely, the R-MCM with uniform structural thickness, the R-MCM with variable structural thickness, and the A-MCM with variable structural thickness, are utilized to form the multiscale structures. The exact mapping methodologies and workflows are detailed in the Supplemental Materials.

3.1.2 Numerical Verification. With a mathematically proven shape-preserving characteristic, how well the R-MCM with uniform thickness is preserving the mapped structure performance is verified in this section. For the performance verification of two other mapping schemes, the process is the same.

The mapped multimaterial multiscale MBB beam structure, as shown in Fig. 3(*b*) is imported into the COMSOL FEA package after proper model cleaning. The Young's modulus for the multiscale structure is 1, which is the same as the structural Young's modulus used for metamaterial topology optimization. The MBB beam multiscale structure is meshed with 2,098,140 triangular elements, and the simulation boundary conditions are the same as Fig. 3(*a*). The 2D example is solved under the plane-stress assumption. The final calculation result is shown in Fig. 3(*d*) with the actual structural strain energy of 86.29. On the other hand, the structural strain energy with the effective material properties after the topology optimization, as shown in Fig. 2, is 72.3898.

It can be noticed that this numerical verification calculation result has higher structural strain energy. This means the FEA model analyzed in Fig. 3(*d*) is less stiff when compared with the optimized structure directly from the optimization. This is due to the information losing during the conformal mapping, CAD model cleaning,
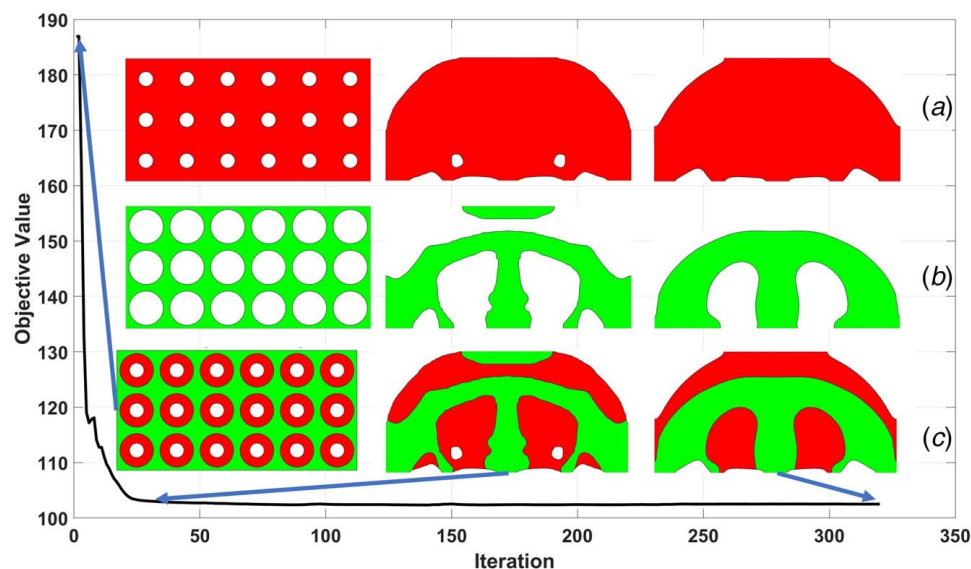

Fig. 4 The evolution history of the Michell-type structure example: (*a*) the evolution history of the first zero-level set function, (*b*) the evolution history of the second zero-level set function, and (*c*) the evolution history of the multimaterial structure. Red: soft material. Green: hard material. (Color version online.)
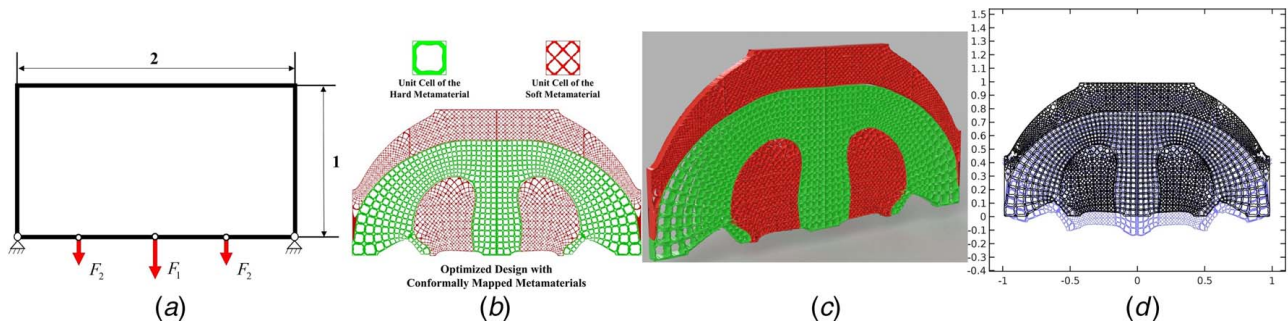
Fig. 5 (*a*) The boundary condition of the Michell-type structure example. (*b*) The R-MCM mapped Michell-type multiscale structure with conformally mapped hard (green) and soft (red) metamaterials. (*c*) The R-MCM mapped Michell-type structure CAD model with uniform thickness. (*d*) The FEA calculation of the R-MCM mapped multiscale michell-type structure with uniform thickness. Black: pre-deformation structure. Blue: post-deformation structure. (Color version online.)

modeling transferring, and other potential reasons discussed previously. But generally, the conclusion can be drawn that the R-MCM with uniform thickness preserves the design material properties in an acceptable manner.

3.2 Simultaneous Optimization of Macroscale Michell-Type Structure and Mesoscale Metamaterials. In this section, the Michell-type structure is designed. With the same optimization setting, the structure topology optimization is carried out with the total volume constraint of 80% and the hard material volume constraint of 40%. The evolution of the design is shown in Fig. 4 with the optimized effective Young's modulus of 0.1 and 0.2 for the soft and hard metamaterial, respectively. The final structure has the total volume of 80% and the hard material volume is 39.992%. The boundary condition is shown in Fig. 5(*a*). The corresponding conformally mapped multiscale structure is shown in Fig. 5(*b*). This model is extruded to be a 2.5D model and is illustrated in Fig. 5(*c*). The structural strain energy with the effective material properties after the topology optimization is 102.5011. In the FEA verification, by using the same boundary condition as Fig. 5(*a*) and 1,285,417 triangular mesh elements, the calculated total strain energy is 121.42 as shown in Fig. 5(*d*).

3.3 Simultaneous Optimization of Macroscale Short Cantilever Beam Structure and Mesoscale Metamaterials. In this section, the short cantilever beam structure is designed within a 1-by-1 design domain discretized into 50×50 elements. The evolution of the design is shown in Fig. 6. The boundary condition is shown in Fig. 7(*a*). With the same material property and the topology optimization settings, the structure topology optimization is carried out with the total volume constraint of 80% and the hard material volume constraint of 40%. The final design has a total volume of 79.972% and the hard material volume of 39.989%, together with the optimized effective Young's modulus of 0.1 and 0.2 for the soft and hard metamaterials, respectively. The corresponding conformally mapped multiscale structure is shown in Fig. 7(*b*). This model is extruded to be a 2.5D model and is illustrated in Fig. 7(*c*). The structural strain energy with effective material properties after the topology optimization is 67.7089. In the FEA verification, by using the same boundary conditions as Fig. 7(*a*) and 1,780,434 triangular mesh elements, the calculated total structural strain energy is 71.12, as can be seen from Fig. 7(*d*).

3.4 The Region-by-Region Multi-Control-Point Conformal Mapping of Variable-Thickness Structures. By using the conformal mapping strategy with variable-thickness structure detailed in the Supplemental Materials, the previous beam examples are
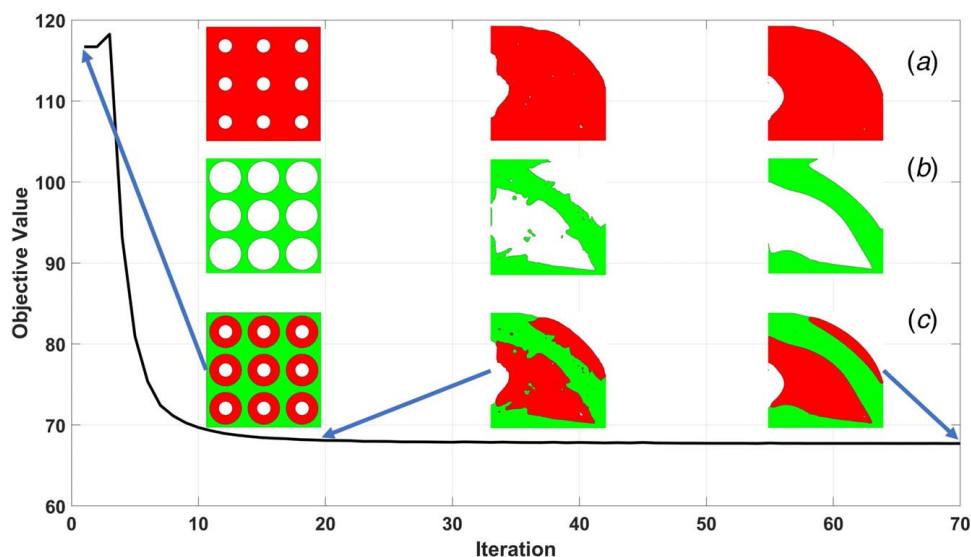

Fig. 6 The evolution history of the short cantilever beam structure example. (*a*) The evolution history of the first zero-level set function. (*b*) The evolution history of the second zero-level set function. (*c*) The evolution history of the multimaterial structure. Red: soft material. Green: hard material. (Color version online.)
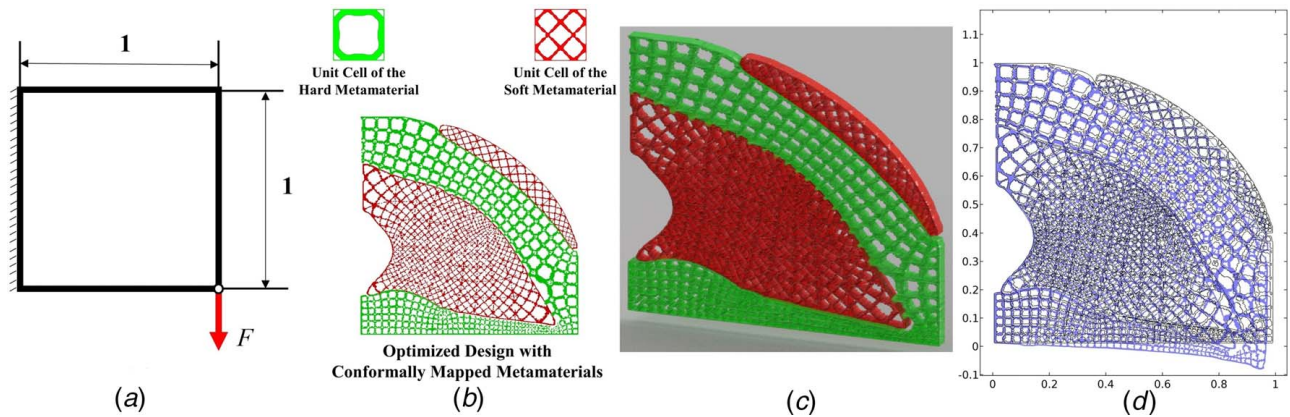
Fig. 7 (a) The boundary condition of the short cantilever beam example. (b) The R-MCM mapped short cantilever beam multiscale structure with conformally mapped hard (green) and soft (red) metamaterials. (c) The R-MCM mapped short cantilever beam CAD model with uniform thickness. (d) The FEA calculation of the R-MCM mapped multiscale short cantilever beam with uniform thickness. Black: pre-deformation structure. Blue: post-deformation structure. (Color version online.)
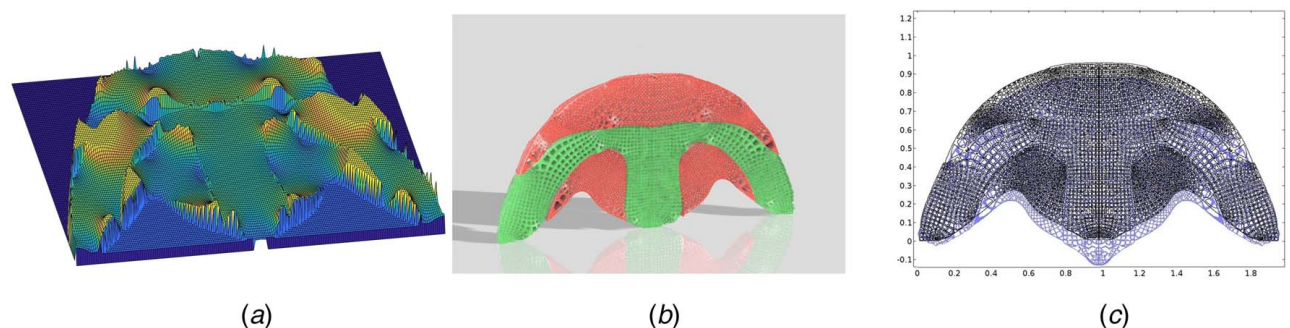

Fig. 8 (a) The thickness value of the R-MCM mapped variable-thickness MBB beam structure. (b) The R-MCM mapped variable-thickness MBB beam structure CAD model. (c) The FEA calculation of the R-MCM mapped multiscale variable-thickness MBB beam structure. Black: pre-deformation structure. Blue: post-deformation structure. (Color version online.)
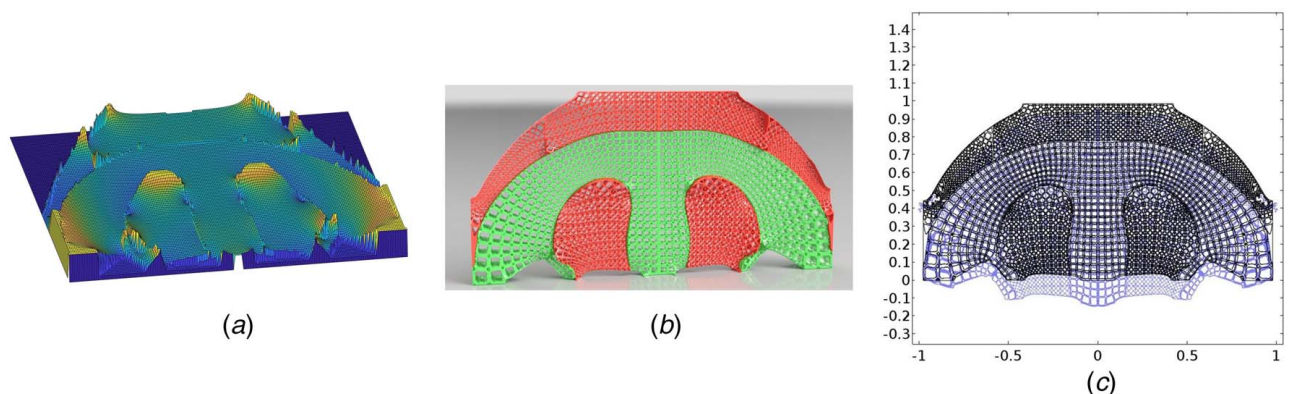

Fig. 9 (a) The thickness value of the R-MCM mapped Michell-type variable-thickness structure. (b) The R-MCM mapped Michell-type variable-thickness structure CAD model. (c) The FEA calculation of the R-MCM mapped multiscale variable-thickness Michell-type structure. Black: pre-deformation structure. Blue: post-deformation structure. (Color version online.)

mapped again, followed by corresponding FEA verification. Each individual material sub-domain is mapped separately, with its own scalar function $e^{2\lambda}$ as the thickness factor. This process is named as R-MCM of variable-thickness structure. In all of the following examples, the thickness value is bounded between 0.5 and 2 times the original thickness. Mathematically, this manually imposed bound might affect the final performance of the mapped structure. But from an engineering point of view considering

manufacturing constraints, this approximation could be considered as acceptable.

The corresponding MBB beam thickness value is shown in Fig. 8(a). By extruding the mapped MBB beam with this thickness value, the variable-thickness MBB beam structure CAD model is shown in Fig. 8(b). It can be seen in Fig. 8(b) that in the areas where the unit cells are stretched, the thickness values are relatively bigger. On the other hand, in the areas where the unit cells are
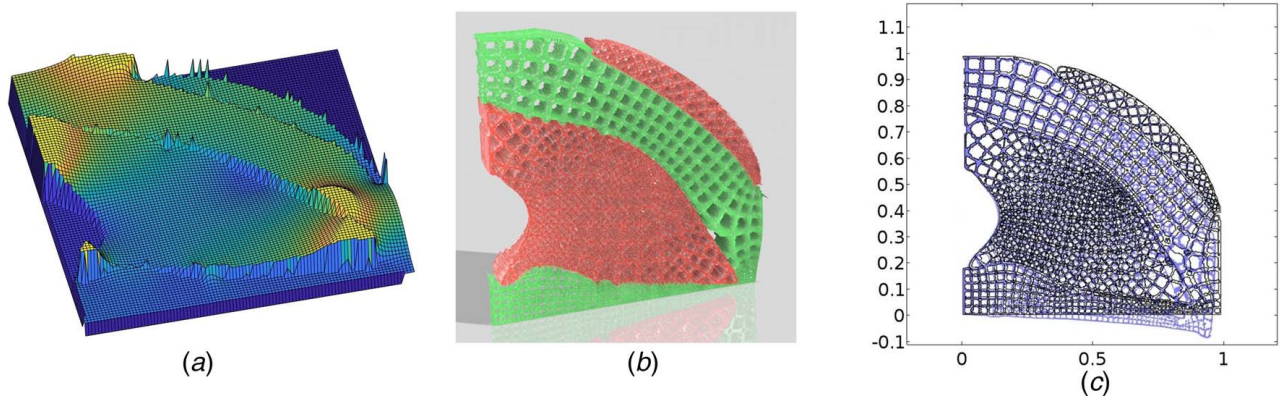
Fig. 10 (*a*) The thickness value of the R-MCM mapped variable-thickness short cantilever beam structure. (*b*) The R-MCM mapped variable-thickness short cantilever beam CAD model. (*c*) The FEA calculation of the R-MCM mapped multiscale variable-thickness short cantilever beam structure. Black: pre-deformation structure. Blue: post-deformation structure. (Color version online.)
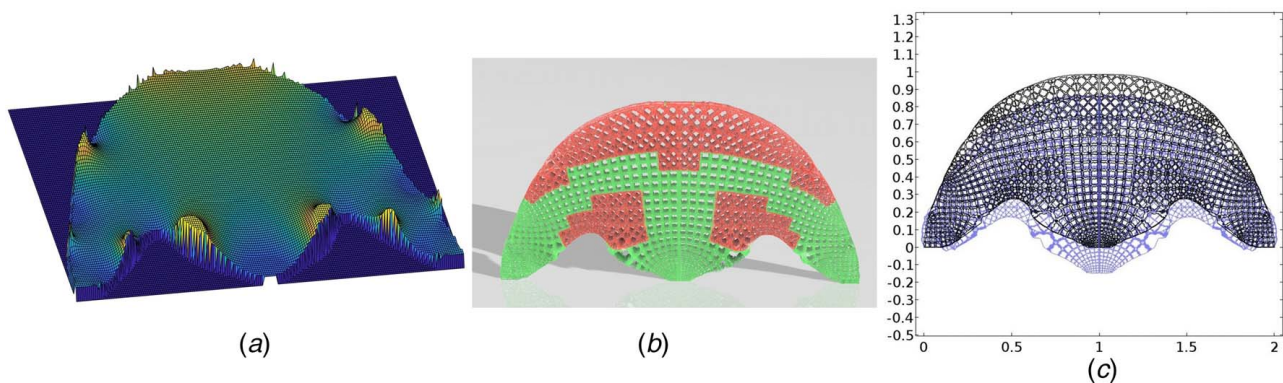

Fig. 11 (*a*) The thickness value of the A-MCM mapped variable-thickness MBB beam structure. (*b*) The A-MCM mapped variable-thickness MBB beam structure CAD model. (*c*) The FEA calculation of the A-MCM mapped multiscale variable-thickness MBB beam structure. Black: pre-deformation structure. Blue: post-deformation structure. (Color version online.)
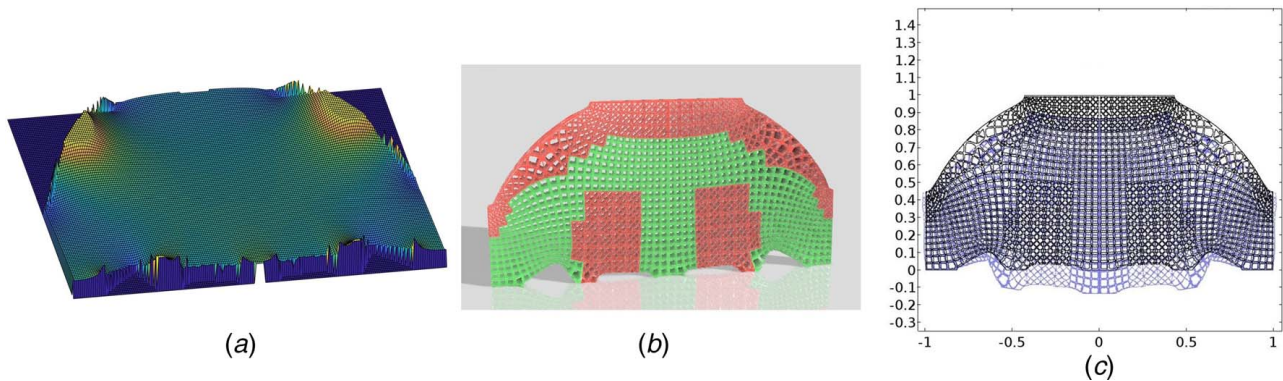

Fig. 12 (*a*) The thickness value of the A-MCM mapped variable-thickness Michell-type structure. (*b*) The A-MCM mapped variable-thickness Michell-type structure CAD model. (*c*) The FEA calculation of the A-MCM mapped multiscale variable-thickness Michell-type structure. Black: pre-deformation structure. Blue: post-deformation structure. (Color version online.)

compressed, the thickness values are reduced accordingly. This is similar to the effects shown in Fig. S9. Relatively, the MBB beam structural stain energy calculated in FEA is 80.74, as shown in Fig. 8(*c*). Similarly, the mapping and FEA analyzing approach are applied to both the Mitchell-type structure and the short beam structure. The thickness values are shown in Figs. 9(*a*) and 10(*a*), and the corresponding CAD models are listed in Figs. 9(*b*) and

10(*b*). The FEA calculations of the structural strain energies are 113.47 and 70.69, respectively, as shown in Figs. 9(*c*) and 10(*c*).

3.5 All-in-One Multi-Control-Point Conformal Mapping of Variable-Thickness Structures. To avoid the drastic thickness change along material interfaces, a novel all-in-one MCM,
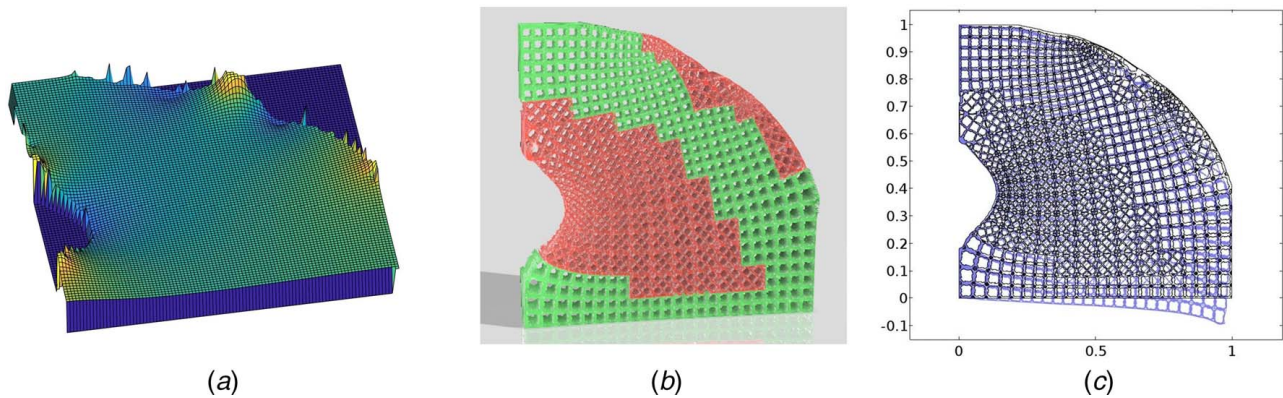
Fig. 13 (a) The thickness value of the A-MCM mapped variable-thickness short cantilever beam structure. (b) The A-MCM mapped variable-thickness short cantilever beam structure CAD model. (c) The FEA calculation of the A-MCM mapped multiscale variable-thickness short cantilever beam structure. Black: pre-deformation structure. Blue: post-deformation structure. (Color version online.)

namely A-MCM mapping is proposed. The detailed mapping process is presented in the Supplemental Materials. With this A-MCM mapping process, the MBB beam, the Michell-type structure, and the short cantilever beam are re-mapped again, followed by FEA structural performance verification. The results are listed below: for the MBB beam, with the thickness value illustrated in Fig. 11(a), the corresponding CAD model is built as Fig. 11(b). By putting this model into COMSOL FEA SOLVER under the same material settings and boundary conditions, the final structural strain energy is 77.41, as seen in Fig. 11(c). For the Michell-type structure, with the thickness value illustrated in Fig. 12(a), the corresponding CAD model is built as Fig. 12(b). The Michell-type structure final structural strain energy is 112.86, as shown in Fig. 12(c). For the short cantilever beam, with the thickness value illustrated in Fig. 13(a), the corresponding CAD model is built as Fig. 13(b). The final strain energy of the short cantilever beam structure is 68.42, as shown in Fig. 13(c).

4 Conclusions and Future Work

In this paper, a concurrent CBF-based PLSM topology optimization framework is proposed for the designing of multimaterial multiscale structures. With the "color" level set representation, multiple material phases are naturally discriminated inside the design domain. By using the CBF to parameterize the level set function, the explicit design variable bounds can be passed to the MMA optimizer. Driven by MMA, the proposed approach can handle multiple constraints and design variables in a straightforward manner. With the help of the local shape-preserving conformal mapping with multiple control points, the designed material properties can be mathematically preserved after the mapping, with the help of the optimized isotropic metamaterials. By introducing the variable-thickness structure, the R-MCM and the A-MCM approaches are proposed to compensate the local metamaterial unit cell distortions. Notably, the A-MCM can map the entire structure in an all-in-one fashion to avoid the drastic thickness change across the material interfaces. Our proposed method is suitable for designing metamaterials for general surfaces, or curved shell structure by a simple extruding operator because the method is based on surface conformal mapping. Nevertheless, this approach can be generalized for designing volumetric metamaterials by replacing the surface conformal mapping by volumetric harmonic mapping, which will be reported in the near future.

Acknowledgment

Conflict of Interest Statement

There is no conflict of interest.

Data Availability

The datasets generated and supporting the findings of this article are obtainable from the corresponding author upon reasonable request. The authors attest that all data for this study are included in the paper. Data provided by a third party are listed in Acknowledgments.

References

[1] Sigmund, O., 2001, "Design of Multiphysics Actuators Using Topology Optimization–Part II: Two-Material Structures," Comput. Methods Appl. Mech. Eng., **190**(49–50), pp. 6605–6627.

[2] Sigmund, O., and Torquato, S., 1996, "Composites With Extremal Thermal Expansion Coefficients," Appl. Phys. Lett., **69**(21), pp. 3203–3205.

[3] Sigmund, O., 2009, "Systematic Design of Metamaterials by Topology Optimization," IUTAM Symposium on Modelling Nanomaterials and Nanosystems, Aalborg, Denmark, May 19–22, pp. 151–159.

[4] Sigmund, O., 1994, "Design of Material Structures Using Topology Optimization," Ph.D. thesis, Technical University of Denmark, Denmark.

[5] Diaz, A. R., and Sigmund, O., 2010, "A Topology Optimization Method for Design of Negative Permeability Metamaterials," Struct. Multidiscip. Optim., **41**(2), pp. 163–177.

[6] Zhou, S., and Li, Q., 2008, "Computational Design of Microstructural Composites With Tailored Thermal Conductivity," Numer. Heat Transfer, Part A: Appl., **54**(7), pp. 686–708.

[7] Zhou, S., Li, W., Sun, G., and Li, Q., 2010, "A Level-Set Procedure for the Design of Electromagnetic Metamaterials," Opt. Express, **18**(7), pp. 6693–6702.

[8] Fullwood, D. T., Niezgoda, S. R., Adams, B. L., and Kalidindi, S. R., 2010, "Microstructure Sensitive Design for Performance Optimization," Prog. Mater. Sci., **55**(6), pp. 477–562.

[9] Deng, J., Yan, J., and Cheng, G., 2013, "Multi-Objective Concurrent Topology Optimization of Thermoelastic Structures Composed of Homogeneous Porous Material," Struct. Multidiscip. Optim., **47**(4), pp. 583–597.

[10] Vlasea, M., Shanjani, Y., Bothe, A., Kandel, R., and Toyserkani, E., 2013, "A Combined Additive Manufacturing and Micro-Syringe Deposition Technique for Realization of Bio-Ceramic Structures With Micro-Scale Channels," Int. J. Adv. Manuf. Technol., **68**(9–12), pp. 2261–2269.

[11] Sigmund, O., and Maute, K., 2013, "Topology Optimization Approaches," Struct. Multidiscip. Optim., **48**(6), pp. 1031–1055.

[12] Allaire, G., Jouve, F., and Toader, A.-M., 2002, "A Level-Set Method for Shape Optimization," Comptes Rendus Mathematique, **334**(12), pp. 1125–1130.

[13] Wang, M. Y., Wang, X., and Guo, D., 2003, "A Level Set Method for Structural Topology Optimization," Comput. Methods Appl. Mech. Eng., **192**(1–2), pp. 227–246.

[14] Sethian, J. A., and Wiegmann, A., 2000, "Structural Boundary Design via Level Set and Immersed Interface Methods," J. Comput. Phys., **163**(2), pp. 489–528.

[15] Yamada, T., Izui, K., and Nishiwaki, S., 2011, "A Level Set-Based Topology Optimization Method for Maximizing Thermal Diffusivity in Problems Including Design-Dependent Effects," ASME J. Mech. Des., **133**(3), p. 031011.

[16] Zhu, B., Zhang, X., and Fatikow, S., 2014, "Level Set-Based Topology Optimization of Hinge-Free Compliant Mechanisms Using a Two-Step Elastic Modeling Method," ASME J. Mech. Des., **136**(3), p. 031007.

[17] Lin, S., Zhao, L., Guest, J. K., Weihs, T. P., and Liu, Z., 2015, "Topology Optimization of Fixed-Geometry Fluid Diodes," ASME J. Mech. Des., **137**(8), p. 081402.

[18] Sethian, J. A., 1996, "Theory, Algorithms, and Applications of Level Set Methods for Propagating Interfaces," Acta Numerica, **5**, pp. 309–395.

[19] Wang, M. Y., and Wang, X., 2004, ""Color" Level Sets: a Multi-Phase Method for Structural Topology Optimization With Multiple Materials," Comput. Methods Appl. Mech. Eng., **193**(6–8), pp. 469–496.

[20] Xia, Q., and Shi, T., 2016, "Optimization of Structures With Thin-Layer Functional Device on its Surface Through a Level Set Based Multiple-Type Boundary Method," Comput. Methods Appl. Mech. Eng., **311**, pp. 56–70.

[21] Wei, P., and Wang, M. Y., 2009, "Piecewise Constant Level Set Method for Structural Topology Optimization," Int. J. Numer. Methods Eng., **78**(4), pp. 379–402.

[22] Merriman, B., Bence, J. K., and Osher, S. J., 1994, "Motion of Multiple Junctions: A Level Set Approach," J. Comput. Phys., **112**(2), pp. 334–363.

[23] Gibson, L. J., and Ashby, M. F., 1999, *Cellular Solids: Structure and Properties*, Cambridge University Press, Cambridge.

[24] Christensen, R. M., 2000, "Mechanics of Cellular and Other Low-Density Materials," Int. J. Solids Struct., **37**(1–2), pp. 93–104.

[25] Valdevit, L., Jacobsen, A. J., Greer, J. R., and Carter, W. B., 2011, "Protocols for the Optimal Design of Multi-Functional Cellular Structures: From Hypersonics to Micro-Architected Materials," J. Am. Ceram. Soc., **94**, pp. s15–s34.

[26] Han, S. C., Lee, J. W., and Kang, K., 2015, "A New Type of Low Density Material: Shellular," Adv. Mater., **27**(37), pp. 5506–5511.

[27] Du, Z., Zhou, X.-Y., Picelli, R., and Kim, H. A., 2018, "Connecting Microstructures for Multiscale Topology Optimization With Connectivity Index Constraints," ASME J. Mech. Des., **140**(11), p. 111417.

[28] Zhou, S., and Li, Q., 2008, "Design of Graded Two-Phase Microstructures for Tailored Elasticity Gradients," J. Mater. Sci., **43**(15), pp. 5157–5167.

[29] Zhou, S., Li, W., Chen, Y., Sun, G., and Li, Q., 2011, "Topology Optimization for Negative Permeability Metamaterials Using Level-Set Algorithm," Acta Mater., **59**(7), pp. 2624–2636.

[30] Wang, Y., Luo, Z., Zhang, N., and Kang, Z., 2014, "Topological Shape Optimization of Microstructural Metamaterials Using a Level Set Method," Comput. Mater. Sci., **87**, pp. 178–186.

[31] Vogiatzis, P., Chen, S., Wang, X., Li, T., and Wang, L., 2017, "Topology Optimization of Multi-Material Negative Poisson's Ratio Metamaterials Using a Reconciled Level Set Method," Comput.-Aided Des., **83**, pp. 15–32.

[32] Wang, Y., Gao, J., Luo, Z., Brown, T., and Zhang, N., 2017, "Level-Set Topology Optimization for Multimaterial and Multifunctional Mechanical Metamaterials," Eng. Optim., **49**(1), pp. 22–42.

[33] Deng, J., and Chen, W., 2017, "Concurrent Topology Optimization of Multiscale Structures With Multiple Porous Materials Under Random Field Loading Uncertainty," Struct. Multidiscipl. Optim., **56**(1), pp. 1–19.

[34] Sivapuram, R., Dunning, P. D., and Kim, H. A., 2016, "Simultaneous Material and Structural Optimization by Multiscale Topology Optimization," Struct. Multidiscipl. Optim., **54**(5), pp. 1267–1281.

[35] Wang, Y., Chen, F., and Wang, M. Y., 2017, "Concurrent Design With Connectable Graded Microstructures," Comput. Methods Appl. Mech. Eng., **317**, pp. 84–101.

[36] Li, H., Luo, Z., Gao, L., and Qin, Q., 2018, "Topology Optimization for Concurrent Design of Structures With Multi-Patch Microstructures by Level Sets," Comput. Methods Appl. Mech. Eng., **331**, pp. 536–561.

[37] Jiang, L., and Chen, S., 2017, "Parametric Structural Shape & Topology Optimization With a Variational Distance-Regularized Level Set Method," Comput. Methods Appl. Mech. Eng., **321**, pp. 316–336.

[38] Luo, Z., Tong, L., Wang, M. Y., and Wang, S., 2007, "Shape and Topology Optimization of Compliant Mechanisms Using a Parameterization Level Set Method," J. Comput. Phys., **227**(1), pp. 680–705.

[39] Wang, S., and Wang, M. Y., 2006, "Radial Basis Functions and Level Set Method for Structural Topology Optimization," Int. J. Numer. Methods Eng., **65**(12), pp. 2060–2090.

[40] Svanberg, K., 2007, *MMA and GCMMA – Two Methods for Nonlinear Optimization*.

[41] Dunning, P. D., and Kim, H. A., 2015, "Introducing the Sequential Linear Programming Level-Set Method for Topology Optimization," Struct. Multidiscip. Optim., **51**(3), pp. 631–643.

[42] Wang, Y., and Kang, Z., 2018, "A Velocity Field Level Set Method for Shape and Topology Optimization," Int. J. Numer. Methods Eng., **115**(11), pp. 1315–1336.

[43] Jiang, L., Ye, H., Zhou, C., and Chen, S., 2019, "Parametric Topology Optimization Toward Rational Design and Efficient Prefabrication for Additive Manufacturing," ASME J. Manuf. Sci. Eng., **141**(4), p. 041007.

[44] Jiang, L., Chen, S., and Jiao, X., 2018, "Parametric Shape and Topology Optimization: A New Level Set Approach Based on Cardinal Basis Functions," Int. J. Numeri. Methods Eng., **114**(1), pp. 66–87.

[45] Jiang, L., Ye, H., Zhou, C., Chen, S., and Xu, W., 2017, "Parametric Topology Optimization Toward Rational Design and Efficient Prefabrication for Additive Manufacturing," ASME 2017 12th International Manufacturing Science and Engineering Conference Collocated With the JSME/ASME 2017 6th International Conference on Materials and Processing, Cleveland, OH, Aug. 6–9, American Society of Mechanical Engineers, p. V004T05A006.

[46] Jiang, L., Chen, S., and Wei, P., 2018, "Concurrent Optimization of Structure Topology and Infill Properties With a Cardinal-Function-Based Parametric Level Set Method," ASME 2018 International Design Engineering Technical Conferences and Computers and Information in Engineering Conference, Quebec City, Canada, Aug. 26–29, American Society of Mechanical Engineers, p. V02BT03A006.

[47] Jiang, L., Guo, Y., Chen, S., Wei, P., Lei, N., and Gu, X. D., 2019, "Concurrent Optimization of Structural Topology and Infill Properties With a CBF-Based Level Set Method," Front. Mech. Eng., **14**(2), p. 171.

[48] Jiang, L., Chen, S., and Gu, X. D., 2019, "Generative Design of Multi-Material Hierarchical Structures via Concurrent Topology Optimization and Conformal Geometry Method," ASME 2019 International Design Engineering Technical Conferences and Computers and Information in Engineering Conference, Anaheim, CA, Aug. 18–21.

[49] Challis, V., Roberts, A., and Wilkins, A., 2008, "Design of Three Dimensional Isotropic Microstructures for Maximized Stiffness and Conductivity," Int. J. Solids Struct., **45**(14–15), pp. 4130–4146.

[50] Radman, A., Huang, X., and Xie, Y., 2013, "Topological Optimization for the Design of Microstructures of Isotropic Cellular Materials," Eng. Optim., **45**(11), pp. 1331–1348.

[51] Guth, D., Luersen, M., and Muñoz-Rojas, P., 2015, "Optimization of Three-Dimensional Truss-Like Periodic Materials Considering Isotropy Constraints," Struct. Multidiscip. Optim., **52**(5), pp. 889–901.

[52] Li, C., Xu, C., Gui, C., and Fox, M. D., 2010, "Distance Regularized Level Set Evolution and Its Application to Image Segmentation," IEEE Trans. Image Process., **19**(12), pp. 3243–3254.

[53] Neves, M., Rodrigues, H., and Guedes, J. M., 2000, "Optimal Design of Periodic Linear Elastic Microstructures," Comput. Struct., **76**(1–3), pp. 421–429.

[54] Zhang, W., Dai, G., Wang, F., Sun, S., and Bassir, H., 2007, "Using Strain Energy-Based Prediction of Effective Elastic Properties in Topology Optimization of Material Microstructures," Acta Mech. Sin., **23**(1), pp. 77–89.

[55] Huang, X., Radman, A., and Xie, Y., 2011, "Topological Design of Microstructures of Cellular Materials for Maximum Bulk Or Shear Modulus," Comput. Mater. Sci., **50**(6), pp. 1861–1870.

[56] Wang, M. Y., Zong, H., Ma, Q., Tian, Y., and Zhou, M., 2019, "Cellular Level Set in B-Splines (CLIBS): A Method for Modeling and Topology Optimization of Cellular Structures," Comput. Methods Appl. Mech. Eng., **349**, pp. 378–404.

[57] Li, H., Luo, Z., Gao, L., and Walker, P., 2018, "Topology Optimization for Functionally Graded Cellular Composites With Metamaterials by Level Sets," Comput. Methods Appl. Mech. Eng., **328**, pp. 340–364.